Investigation of Magnetic Properties of #-Fe203 NP-Decorated Carbon Nanostructured Mats

Investigation of Magnetic Properties of γ-Fe_2O_3NP-Decorated Carbon Nanostructured Mats

Cite this article as: Hammad Younes, Md Mahfuzur Rahman, George Ni, Amal Al Ghaferi, Rashid Abu Al Rub and Ibrahim Bsoul, Investigation of Magnetic Properties of γ-Fe_2O_3NP-Decorated Carbon Nanostructured Mats, JOM https://doi.org/10.1007/s11837-019-03631-4

Investigation of Magnetic Properties of ɤ-Fe_2O_3 NPs Decorated Carbon Nanostructured Mats

Hammad Younes [a*], Md Mahfuzur Rahman [b**], George Ni[c], Amal Al Ghaferi [a], Rashid Abu Al Rub [a], and Ibrahim Bsoul[d]

[a] Department of Mechanical and Material Engineering, Masdar Institute of Science and Technology, Khalifa University of Science and Technology, P.O box 54224, Abu Dhabi, United Arab Emirates.
[b]Department of Industrial and Production Engineering (IPE), Military Institute of Science and Technology (MIST), Mirpur, Dhaka, Bangladesh.
[c]MIT Lincoln Laboratories, Massachusetts Institute of Technology, 77 Massachusetts Ave, Cambridge, Massachusetts 02139.
[d] Department of physics, Al al-Bayt University, P.O.BOX 130040, Mafraq 25113, Jordan.

Abstract

It has been experimentally demonstrated that a carbon nanostructure (CNS) based structure, called CNS mats, can yield superior magnetic properties. The structure is obtained by decorating CNS with ɤ-Fe_2O_3 nanoparticles (NPs) in a 3D network structure. ɤ-Fe_2O_3 NPs are coated on the CNS resulting in enhanced magnetic properties. The experimental characterization and theoretical analysis reveals that the CNS mats decorated with ɤ-Fe_2O_3 NPs show superior magnetic properties compared to pristine CNS, as a result of the homogeneous dispersion of ɤ-Fe_2O_3 NPs and the highly aligned structure of CNS. The coercive field (Hc), saturation magnetization (Ms) and the remnant magnetization (Mr) were found to be 126 Oe, 22.3 (emu/g) and of 7.15 (emu/g) respectively. In addition, SEM and AFM characterization show that the CNTs in each CNS flake within the CNS mat remained well aligned and form an interconnected 3D network structure. This results in a robust porous structure with high electrical conductivity. Thermogravimetric Analysis (TGA) reveals that the presence of the ɤ-Fe_2O_3 NPs provides a protection layer for the CNS and results in good thermal stability. The fabricated ultra-thin CNS mat offers superior magnetic and electrical performance that makes it an attractive candidate for microwave absorption, along with other application such as electromagnetic shielding, sensors, lithium ion battery and polymer composites.

Keywords: Carbon Nanostructured Mats, Magnetization property, Electromagnetic wave absorber, 3D network structure.

*Corresponding author. Hammad Younes Tel.: +971-2810-9319; Fax: +971-2810-9901
E-mail address: Hammad.Younes@ku.ac.ae,
**Corresponding author Md. Mahfuzur Rahman Tel: +8801794061876
E-mail address: mahfuz.ipe@gmail.com

1. Introduction

Since the discovery of carbon nanotubes (CNTs) in 1991[1], extensive research efforts have been invested to study their unique structural, electrical, optical, mechanical and thermal properties [2-8] with the aim of extending their application in various technology fields. Numerous potential applications have been reported by blending the electrical properties of CNTs with the magnetic properties of metal[9-18]. It includes electromagnetic interference shielding (EMI SH), high-density magnetic data storages, magnetic nanofluids, heterogeneous catalysis, biomedical, microwave absorption and biotechnological applications through magnetically guided drug delivery systems. Recently, magnetic CNT composites have attracted much attention, as unusual magnetization has been observed in CNT based buckypaper film[17,19,20]. Composites of CNTs and magnetic materials exhibit ferromagnetic behavior, which differs from the superparamagnetic properties in iron oxides filled CNTs [21,22]. In particular, CNTs filled with ferromagnetic Fe-based crystals like Fe_3C, α-Fe, FeCo, FeNi, CoNi, Co and Ni crystals have been shown to be the most effective method for enhancing saturation magnetization in buckypaper [17,18,20,23]. Despite successful enhancement of saturation magnetization using Fe-filled CNTs, the method of filling a remarkably small inner cavity in CNTs using capillary filling [7,8] and chemical vapor deposition[18,24] is quite complex and expensive. Therefore, a simple and economically viable process is needed to enhance saturation magnetization of buckypaper. A simple and scalable method has been reported for the fabrication of CNT-based strong paper sheet through ultrasonicated dispersion and vacuum filtration, and it can be used to to fabricate CNS mats decorated with magnetic materials [25]. In this method, effective dispersion of CNTs in water is the key for efficient decoration with magnetic nanoparticles.

Dispersing SWNTs in water is very difficult owing to their hydrophobic nature and the formation of tight bundles caused by very strong Van der Waals attraction forces, which can be in the order of 500 eV per micrometer of tube contact. Therefore, a combination of physical and chemical methods are used to prevent formation of CNTs bundles [26]. Physical methods require ultrasonicators to provide sufficient energy to physically separate nanotubes in order to obtain homogenous dispersions. Chemical methods for effective dispersion of CNTs can involve covalent or non-covalent modifications. For example, the treatment of CNTs in strong acids attaches a hydrophilic functional group to CNT walls, resulting in covalent modification. Although covalent modification produces good dispersion, over modification via oxidation

causes fragmentation and shortening of the CNTs, which negatively affects their thermal, electrical and mechanical properties. To overcome these issues, researchers turned into exploring non-covalent modifications by using surfactants. A uniform dispersion of CNTs can be made possible by taking advantage of the amphiphilic nature of these molecules. In this approach, the hydrophobic part of the surfactant adheres to the CNT sidewalls, while the hydrophilic part aids in the solubility. Islam et al [27] clarified the mechanism of stabilizing CNTs using surfactants. The surfactants cover the surface of the CNTs forming a hemimicellular shape, by which the hydrophilic head of the surfactant creates a compact outer surface, while the hydrophobic tail of the surfactant remains in contact with the nanotube walls. In addition, the binding energy between the CNTs and the surfactant is significantly enhanced due to the π- interaction between the benzene ring of the surfactant and the surface of the CNTs. Moreover, the repulsion between the sulfonic groups on the surfactant improves the debundling of the CNTs as seen in Fig. 1(a). The surfactant SDBS dissociates in water into two parts, as described in Fig. 1(a). The sulfonic group carries negative charge, whereas the sodium ions carry positive charge [28]. The presence of positive and negative charges is crucial for the effective decoration of iron oxide nanoparticles on CNTs.

As mentioned before, the hydrophobic surfactant tails are adsorbed at the surface of the carbon nanotubes, whereas the head, which carries a negative charge, attracts the iron oxide nanoparticles, which have a partially positive charge. The carbon nanotubes solution has a pH of 6.15, at which the magnetic sensitive ɤ-Fe_2O_3 nanoparticles have a positive zeta potential charge Fig. 1(b). The positive ɤ-Fe_2O_3 NPs interact and adhere electrostatically to the negative charge on the sulfonic group.

Several approaches have been reported for the fabrication of CNT-based nanocomposites in a variety of applications [10-12,29-37]. Kim et al. [38] described a method of making magnetic-sensitive carbon nanotubes using a single reaction approach between MWCNT-COOH and Fe $(NO_3)_3.9H_2O$ with a simple modified sol–gel technique. The fabricated magnetic-sensitive carbon nanotubes were used to prepare magnetic-sensitive MWCNT/epoxy composites with high electrical conductivity. Greg et al. [39] used nonionic surfactants (Triton X-100) to tether ɤ-Fe_2O_3 NPs to single wall carbon nanotubes functionalized with polyethylene glycol (SWNT-PEG). The results showed that Triton X-100 helps to obtain a high degree of dispersion of the Fe_2O_3 and SWNT. In addition, alignment in an external magnetic field was clearly observed for an aqueous

dispersion of Fe_2O_3 and SWNT. Younes et al. [40] fabricated magnetic-sensitive carbon nanofibers for nanofluids applications. Gao et al. [41] explored biomedical applications by decorating CNTs with Fe_3O_4, which electrostatically assembled on the surface of sheep red blood cells. The blood cells that tethered to the magnetic CNTs were able to be manipulated via external magnetic fields. Yuqing et al. [42] fabricated magnetic composites containing polyaniline, strontium ferrite, and MWNTs, and studied the composite electromagnetic properties. By using 2.0 g of MWNTs the electrical conductivity of the polymer nanocomposites was found to be 7.2196 S/cm whereas the coercive force was found to be 7457.17 Oe. The exceptional electromagnetic properties showed that the composites could be used as microwave absorbers. Guan et al. [43] used magnetic MWNTs in biomedical applications by extracting estrogen using magnetic MWNTs. A sol-gel method was used to fabricate magnetic silica particle-coated MWNTs. Lei et al. [44] used a chemical deposition method to decorate CNTs with Fe_3O_4 NPs. The Fe_3O_4-decorated CNTs were used to separate pyrethroids from tea samples. Gonnet et al. [12] used very high magnetic fields to align SWNTs. He fabricated aligned SWNTs buckypaper and epoxy composites. There was no improvement on the thermal conductivity of the epoxy composites, but the thermal conductivity of the buckypaper was enhanced to 42 W/mK.

Analyzing the reported studies referenced above, it is observed that few reports focused on the fabrication of magnetic sensitive CNTs mats with high electrical conductivity [12]. Moreover, most of the reported studies in the literature are either about the fabrication of magnetic-sensitive CNT powder or magnetic-sensitive CNT polymer (nanocomposites) that are used in different applications such as in catalysis, electronic devices, sensors and magnetic applications. The origin of these unusually low saturation magnetizations is still an open problem that limits the translation of these nanostructures to key applications. Therefore, these materials needs to be further explored for enhanced magnetic properties.

In this paper, we address the fabrication of freestanding and flexible magnetic sensitive CNS mat through a cost-effective and reproducible technique by focusing on the decoration of carbon nanostructures (CNS) with γ-Fe_2O_3 NPs. CNS is a novel carbon-based material developed by a group of scientists at Applied Nanostructured Solutions, LLC (ANS), a Lockheed Martin Corporation company. In CNS, relatively long carbon nanotubes are grown on fiber

substrates in one direction and bundled in flake shaped form. [45] . These CNS, which have superior structural and conductive properties, have been used to fabricate magnetic-sensitive CNS mats with very high electrical conductivity and great electromagnetic absorption properties. The incorporation of ɤ-Fe_2O_3 NPs don't alter the intrinsic alignment and network structure of the CNS, which has been verified through morphological studies using scanning electron microscope (SEM) and atomic force microscope (AFM). Uniform coating of ɤ-Fe_2O_3 NPs has been obtained using surfactants as a linking material between ɤ-Fe_2O_3 NPs and CNTs. In addition, Energy Dispersive X-ray (EDX) and XPS spectroscopy have quantified the effective decoration of CNS using ɤ-Fe_2O_3 NPs. Moreover, Raman spectroscopy has been used to understand how ɤ-Fe_2O_3 nanoparticle decoration affects the CNS materials. Vibrating-Sample Magnetometer (VSM) tests have been carried out to quantify the magnetic properties of the CNS Mats. The fabricated CNS mats have the potential to offer superior magnetic and electrical performance, yet is compact, lightweight, and cost-effective. The fabricated mats can be used in different technologies such as electromagnetic interference shielding, wearable devices and biomedical applications.

2. Material and Methods

2.1. Material and Instruments

The magnetic sensitive CNS mats were fabricated using CNS materials obtained from Applied Nanostructured Solutions, LLC CNS. The CNS materials arrive in flakes shape with different widths and 300-350 µm length. Sodium dodecylbenzenesulfonate (SDBS) and γ-Fe_2O_3 NPs (diameter of 25–50 nm) were purchased from Sigma-Aldrich. The CNS and the γ-Fe_2O_3 NPs were dispersed using a Qsonica model Q 500 (500 watts). The magnetic properties were measured at Al al-Bayt University, Mafraq, Jordan using a vibrating sample magnetometer (VSM) at room temperature with 15,000 Oe maximum applied field. The SEM images were taken using an FEI Nova NanoSEM 650. The TEM images were taken using an FEI Tecnai 200 kV G2 series TEM. The atomic force microscopy (AFM) images and data have been obtained using an Asylum MFP-3D tool, with 500 V applied voltage, 1.5 V deflection and 0.7 Hz scan speed. The alpha 300 R WITec's Confocal Raman was used to obtain Raman spectra. Raman spectra were obtained with a green laser (excitation energy E_{exc}=2.33 eV). An Instron machine

model 5982K9102 was used to measure the mechanical strength. A Lake Shore Hall Effect Measurement (HMS) systems, model 7700 A was used to measure the electrical conductivity for the CNS mats. BET analysis was done using a Quantachrome NOVA 2000e gas sorption system, and XPS analysis was performed using a KRATOS system equipped with an Al K 1486.6 eV source gun, which produced a 400-μm spot size in the standard lens mode.

2.2. Methods

The CNS fabrication is described in **Fig. 1c**. The CNS materials were dispersed in water using a tip ultra-sonicator, and then the solution was filtered using a vacuum filtration method. The methods can be found in details in reference [46].

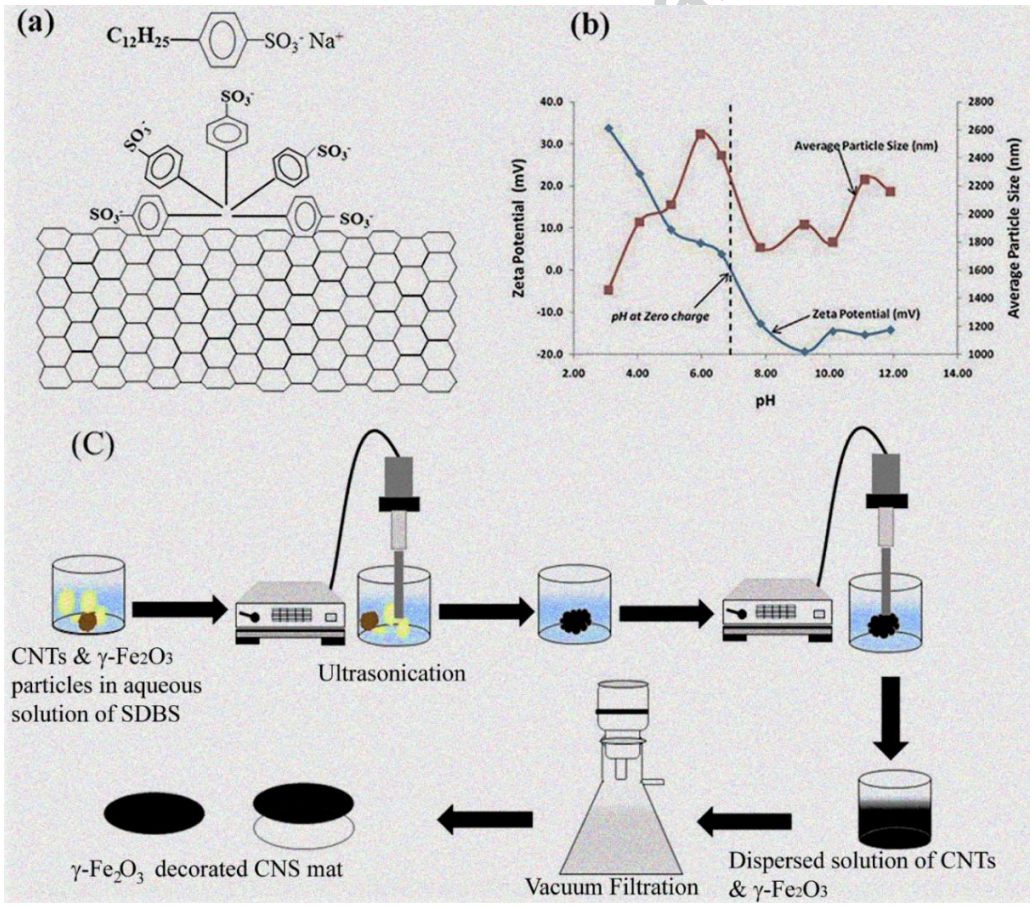

Fig. 1 (a) A schematic diagram showing the dissociation reaction and the interaction of SDBS in aqueous solution with CNTs (b) Zeta potentials of ɤ-Fe_2O_3 particles in aqueous solution showing average particle size versus different pH values (Reprinted with permission from reference[[47]]). (c) Preparation method for the CNS mats.

3. Results and Discussion

3.1 Material Structure

A robust material structure for the composite of CNTs and magnetic materials towards obtaining superior magnetic and electrical performance requires to possess numerous characteristics. These are better thermal and electrical conductive properties, absence of magnetic material by-products, optimum quantity of Fe present within the CNTs for enhanced magnetization properties, high magnetic coercivities, lightweight and high flexibility, small thickness, and an interconnected structure of CNTs to form a network structure. Carbon-based porous materials provide competitive advantages due to lower weight and cost for applications such as microwave-absorption. Higher porosity and lower density can lead to strong microwave absorption capacity by allowing multiple reflections on CNT wall interfaces. To achieve these characteristics, we used the vacuum filtration method after dispersing the CNTs and γ-Fe_2O_3 NPs in an aqueous solution of SDBS. The process is depicted in **Fig. 1c**. The proper dispersion of CNTs is vital to the effective creation of freestanding, flexible, and foldable carbon nanostructure (CNS) mats with superior alignment, density and magnetic sensitivity. In addition, proper dispersion plays an important role in understanding how ɤ-Fe_2O_3 NPs can decorate the outer surface of the CNS.

3.2 Structures and Properties of magnetic sensitive CNS mat

The morphology of CNS and ɤ-Fe_2O_3 NPs was characterized by SEM and TEM in **Fig. 2**. The CNS flakes consist of CNTs that are intrinsically aligned with a length between 300-400 µm as shown in **Fig. 2a**. This alignment provides channels for ballistic electron transport and improves the electron electrical conductivity of the material. In addition to the directional alignment, CNTs in a CNS flake are interconnected to each other, forming a network structure, shown in **Fig. 2b**, that improves the robustness of the composite of CNTs and magnetic materials. From the TEM images **(Fig. 2b)** of the CNS, it is obvious that CNTs (diameter ~15-

25nm) are entangled with each other. CNS flakes are considered non-magnetic material due to poor magnetic sensitivity. Therefore, ɤ-Fe_2O_3 NPs have been embedded into the non-magnetic CNS material by blending them together through dispersion to integrate all the unique characteristics of CNTs with the magnetic properties of NPs. From the TEM images of the ɤ-Fe_2O_3 NPs **(Fig. 2c)**, the average size of NPs lies in the range of 25-50 nm. ɤ-Fe_2O_3 NPs are hexagonal crystals as the equally spaced lattice fringes is clearly seen (inset of **Fig. 2c**) and the lattice fringes are separated by a distance of 0.37 nm. Diffraction pattern obtained from TEM analysis (**Fig. 2d**) further confirms the crystalline properties of the ɤ-Fe_2O_3 NPs.

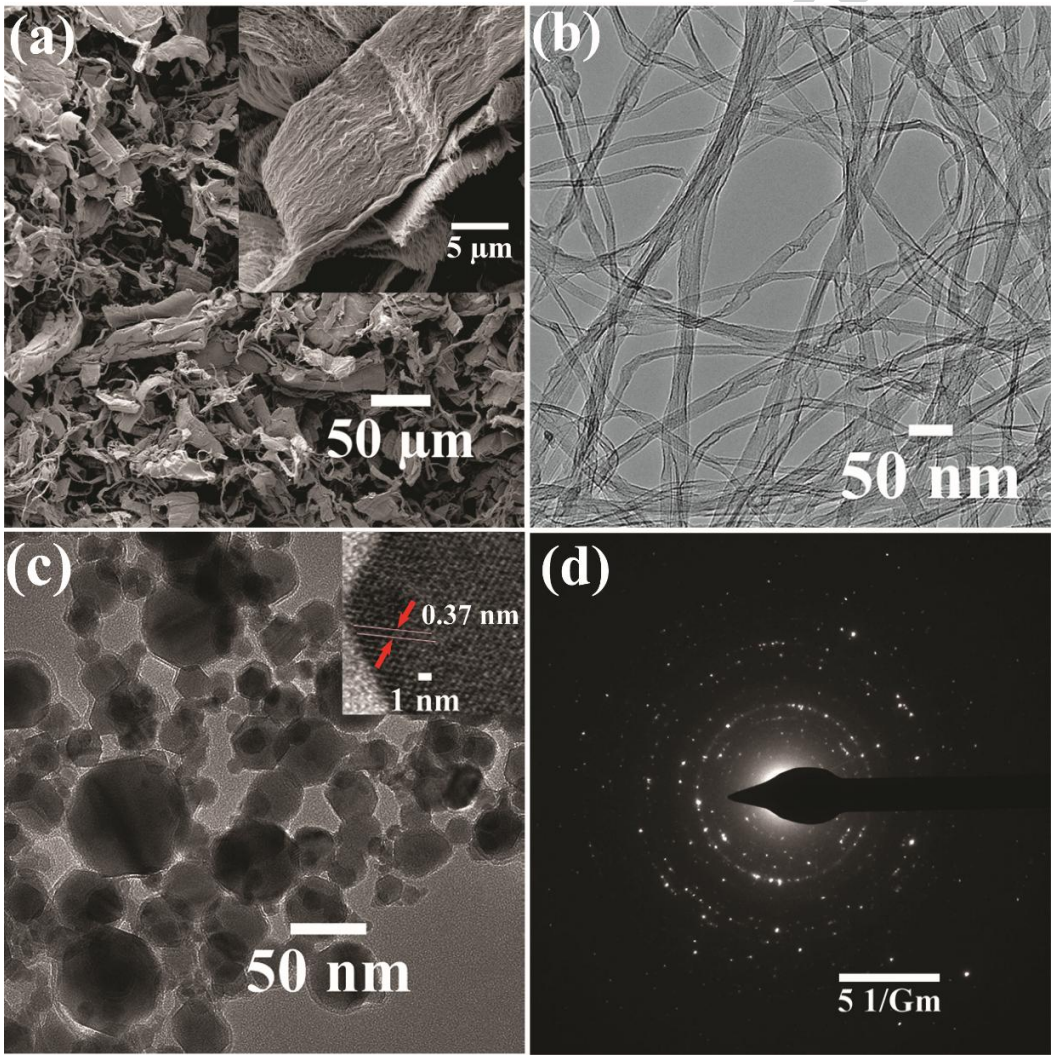

Fig. 2 Structural and morphological characterization of CNS flakes and ɤ-Fe_2O_3 NPs. (a) SEM image shows many CNS flakes and the inset shows one CNS flake , (b) High-resolution TEM

images showing CNS. (c) Low magnification TEM image of ɤ-Fe_2O_3 NPs (d) Diffraction pattern obtained from TEM analysis and it shows the crystalline properties of the ɤ-Fe_2O_3 particles.

The structural and morphological features of the as-fabricated freestanding, flexible and foldable pristine CNS mat and the CNS mat decorated with ɤ-Fe_2O_3 NPs were first revealed using SEM analysis (**Fig. 3**). The SEM images of the CNS mat show an interconnected 3D network consisting of directionally oriented CNTs skeleton, whose surface is uniformly porous and flat (**Fig. 3a & 3b**). The AFM analysis further confirmed the interconnected 3D network structure with aligned CNTs, during the fabrication of CNS mat (**Fig. 4a & 4b**). The EDX analysis (**Fig. 3c**) showed the presence of expected Fe metal content to achieve superior magnetic properties. EDX spectrum confirmed that the sample has 56 wt% Carbon, 31 wt% Iron, and 10 wt% oxygen. The presence of Na and S peaks are because of using a surfactant (NaDDBS) with sodium and sulfonate. The flexibility of the as fabricated CNS mats are shown in the camera image **Fig. 3d**. A high degree of flexibility is observed in the developed structure, and the mats can be shaped in different ways so that these can be easily incorporated into wearable and foldable devices.

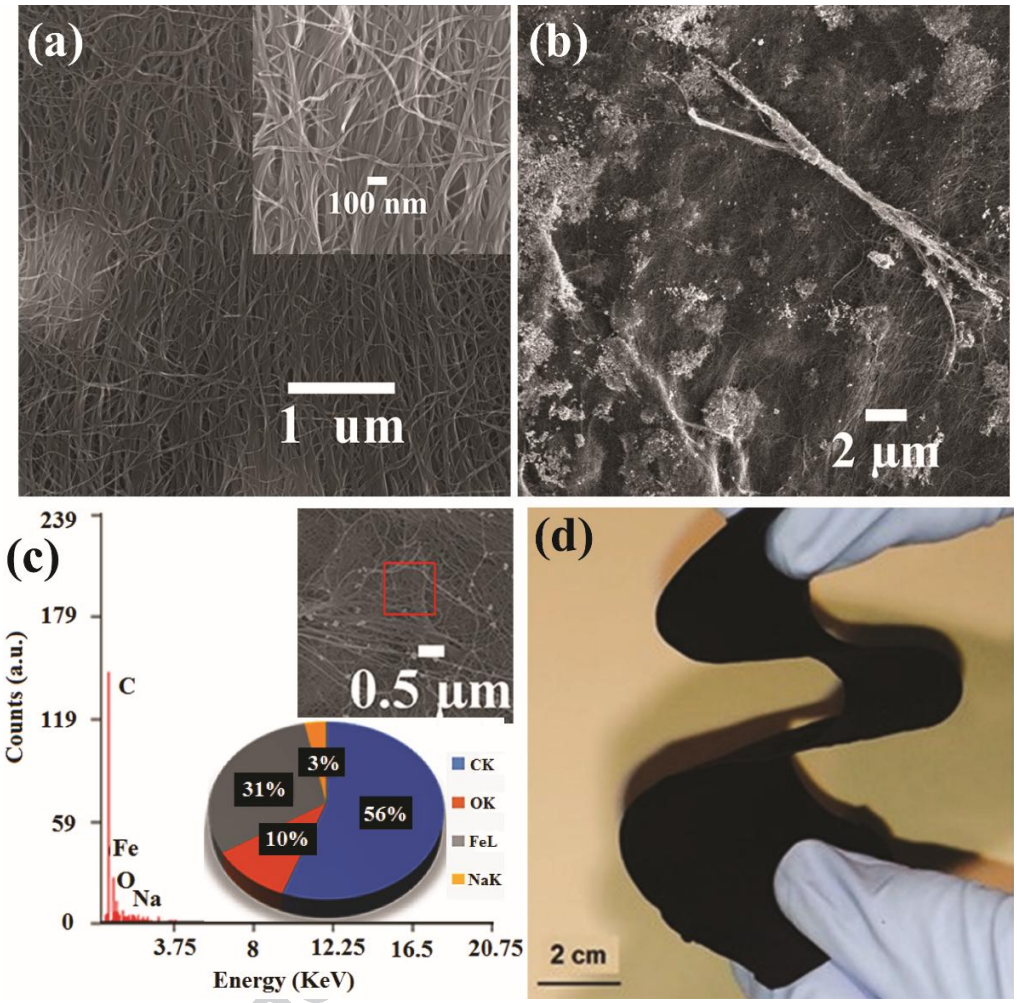

Fig. 3 Structural and morphological characterization of as synthesized CNS Mats. (a) SEM image of the surface of CNS mats without Fe_2O_3 NPs, (b) SEM image of the surface of CNS mats decorated with ɤ-Fe_2O_3 NPs, (c) EDX spectrum of Carbon nanostructures decorated with ɤ-Fe_2O_3 NPs and, (d) Camera images showing the flexible magnetic sensitive CNS mat.

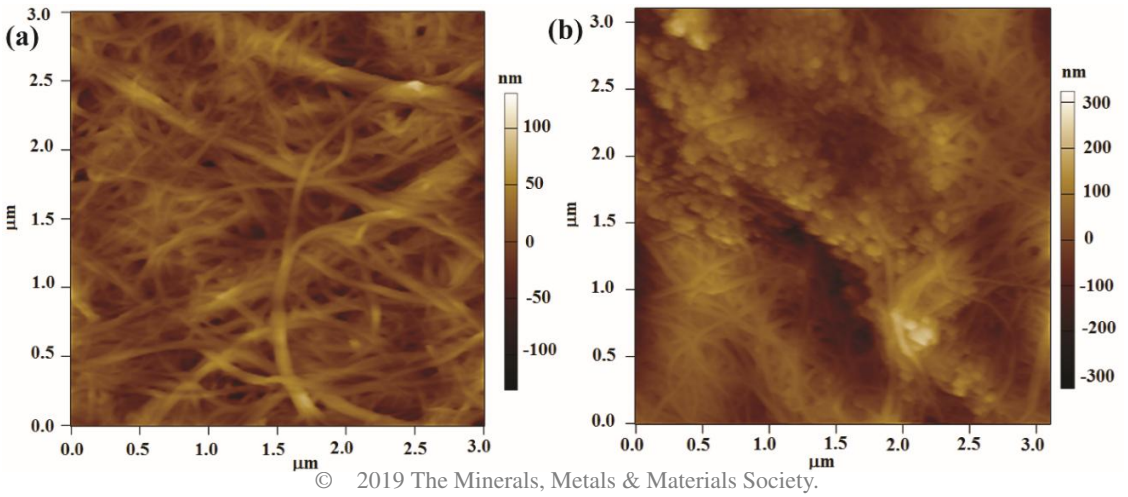

Fig. 4 AFM characterization of the CNS mat for the determination of CNS orientation and the interconnected 3D network structure. (a) Shows the topography of a pristine CNS mat and (b) shows the 3D network structure of the ɤ-Fe_2O_3 NPs decorated CNS mat. Images are obtained through the non-contact mode AFM.

The developed structure possesses a fairly good degree of alignment in the nanoscale, as confirmed by SEM (**Fig. 3**) and non-contact mode AFM analysis (**Fig. 4**). This alignment of the CNS in the nanoscale plays a crucial role in providing high electrical conductivity, as it creates conduction paths for ballistic electron transport. Moreover, the structural properties of the CNS mats were examined using X-ray photoelectron spectroscopy (XPS). The XPS survey spectrum of CNS mat is displayed in **Fig. 5a**. The predominant peaks locating at 713 and 725 eV correspond to the Fe ($2p_{3/2}$) and Fe ($2p_{1/2}$) spin orbit peaks, respectively [48]. It also shows peaks for carbon and oxygen. In addition, the presence of CNTs within the CNS was confirmed through Raman spectra. Raman spectra of (1) CNS powder, (2) as-fabricated CNS mats and (3) CNS mats decorated with ɤ-Fe_2O_3 NPs are shown in **Fig. 5c**. This analysis revealed the presence of G band in the range of 1565-1600 cm^{-1} for the C-C bond in plane vibration and D band at about1351 cm^{-1} due to the presence of disorder in carbon systems. A decrease in the I_D/I_G ratio from 1.06 to 0.65 is observed, due to the removal of impurities during ultra-sonication and washing.

3.3 Thermal stability of ɤ-Fe_2O_3 NPs decorated CNS mat and BET analysis

The thermal stability of the fabricated CNS mats in high temperatures has been investigated through thermo-gravimetric analysis (TGA) and the results are shown in **Fig. 5d**. It is observed that pristine CNS starts to have a thermal degradation at 500 ^oC as most carbon materials burned off in the temperature range of 500-700 ^oC, leaving behind the impurities in the CNS. However, for CNS mats, once temperature is increased above 150 ^oC, a gradual weight loss has been observed and can be attributed to the evaporation of the SDBS surfactant and some moisture. The ɤ-Fe_2O_3 NPs decorated CNS mat exhibits enhanced thermal stability with reduced weight loss (12%), compared to the weight loss of pristine CNS mats (20%). The presence of the ɤ-Fe_2O_3 NPs provides a coating for the CNS that protects them from thermal degradation.

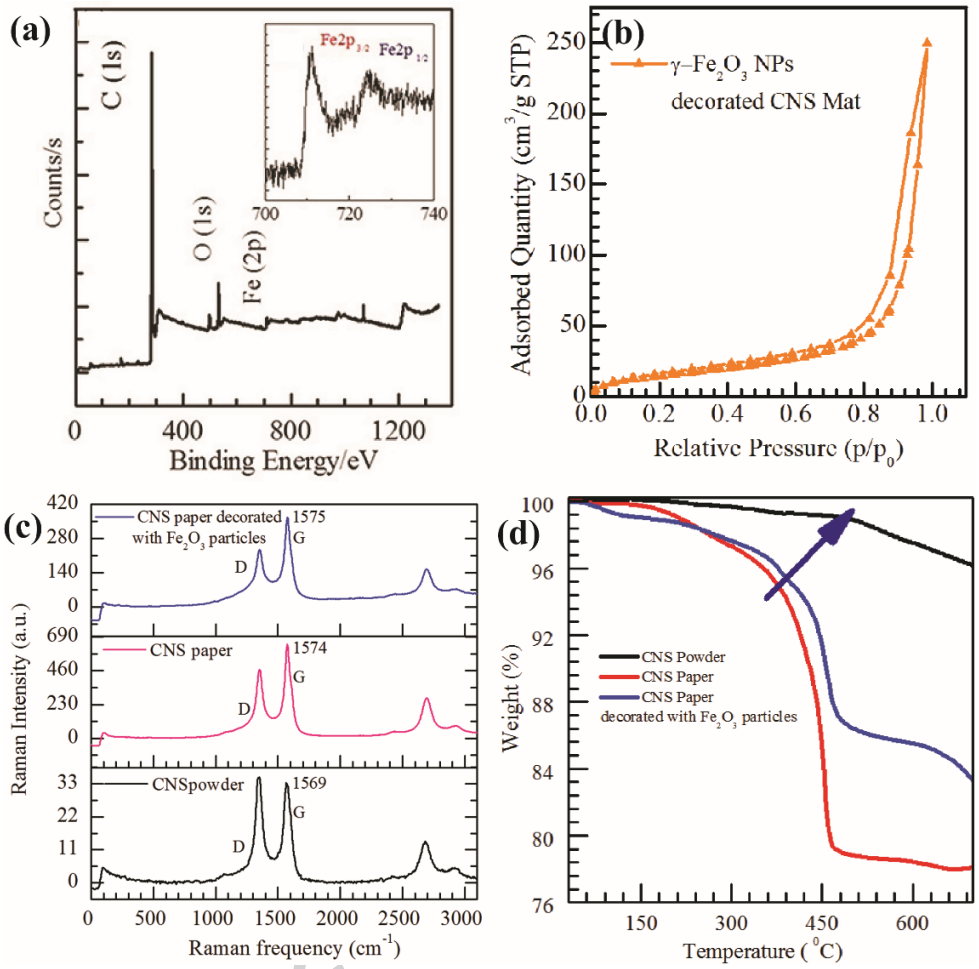

Fig. 5 (a) The X-ray photoelectron spectroscopy spectrum of ɤ-Fe_2O_3 NPs decorated CNS mats, and the inset shows a high-resolution XPS spectrum of iron (2p) bands of the ɤ-Fe_2O_3 NPs decorated CNS mat. (b) Nitrogen adsorption-desorption isotherm of ɤ-Fe_2O_3 NPs decorated CNS mat. (c) Raman spectra of as-fabricated CNS mat and (d) is the Thermogravimetric analysis of pristine CNS powder, CNS mat and ɤ-Fe_2O_3 NPs decorated CNS mat, showing weight loss and differential curves at a heating rate of 10°C/min in nitrogen atmosphere.

Furthermore, Brunauer-Emmett–Teller (BET) analysis was performed on the CNS mat to validate the 3D network structure and the undisturbed intrinsic alignment of CNS. The N_2 absorption/desorption isotherms received at 77.35 K is shown in **Fig. 5b,** suggesting the absorption process to be of type-V in nature, which validates the densely packed but porous structure of CNS mats. According to nitrogen adsorption and desorption measurements, the CNS mats possess low BET specific surface areas of 55.8 m^2/g and the DFT (Density Functional Theory) calculated total pore volume of 0.0263 cm^3/g (**Fig. 5b**) signifying that the CNTs are directionally oriented in the form of a 3D network structure, which are also confirmed by the

SEM and AFM analysis. The inherent interconnected structure of CNS and the formation of better conductive networks among CNTs in the developed structure contributes to better electrical conductivity, which for the pristine CNS mat is as high as 238 S/cm (**Fig. 7a**). After decorating CNS with γ-Fe_2O_3 NPs, a slight decrease in electrical conductivity is observed (**Fig. 7a),** and this can be realized due to the low concentration of NPs. The high electrical conductivity of CNS is due to the highly oriented CNTs, which contribute to ballistic electron transport. In contrast, potential entanglement could cause scattering of electrons, resulting in lower electrical conductivity [46]. According to **Fig. 3 & Fig. 4**, a 3D network structure provides paths for electron conduction through CNTs-CNTs interaction within the structure, or the interaction between the neighbors CNS through their contact giving rise to high electrical conductivity.

The electrical conductivity and magnetic properties of the CNS mat material play important roles in determining performance for many applications, such as electromagnetic shielding performance. Electrical conductivity is required to absorb electromagnetic radiation. Hence, it is of paramount importance for electromagnetic shielding effectiveness of the γ-Fe_2O_3 decorated CNS mats.

3.4 Magnetization of CNS Mats

To confirm the enhanced magnetization of ɤ-Fe_2O_3 NPs decorated CNS mats, a controlled investigation of magnetic properties was carried out through Vibrating-Sample Magnetometer (VSM) tests, and the results are illustrated in **Fig. 6**. The VSM test was performed at room temperature in plane configurations with a maximum field of 2500 Oe, in steps of 5 Oe on three samples, including (i) ɤ-Fe_2O_3 NPs, (ii) pristine CNS mats, and (iii) ɤ-Fe_2O_3 NPs decorated CNS mat. Magnetic parameters of different samples obtained from the magnetization (M) versus applied magnetic field (H) plots for pristine CNS mats and the ɤ-Fe_2O_3 NPs coated CNS mats presented in **Fig. 6** are shown in Table I. Comparison of the results obtained from

these three samples revealed that pure ɤ-Fe_2O_3 didn't saturate even at a 4000 G (Gauss) magnetic field, and showed a narrow hysteresis loop with M_S (saturation magnetization) value of 71 emu/g (at 5000 G) which is much higher than the M_S value (0.23 emu/g) of pristine CNS mats. However, incorporation of ɤ-Fe_2O_3 NPs within the CNS matrix resulted in a 69% reduction in M_S value of ɤ-Fe_2O_3 NPs decorated CNS (22.3 emu/g). This can be attributed to the screening effect of CNTs in CNS, causing a reduced magnetization of ɤ-Fe_2O_3 NPs within the CNS matrix. The enhanced magnetization of ɤ-Fe_2O_3 NPs coated CNS mats can be associated to the presence of Fe within the CNS network. Indeed the saturation magnetization of CNS mats is expected to increase with the optimum loading of ɤ-Fe_2O_3 NPs. As fabricated CNS mat contains 5 wt% of ɤ-Fe_2O_3 NPs, 0.0013 g of ɤ-Fe_2O_3 NPs was added to 0.25 g of CNS, giving rise to the best electrical properties along with the enhanced magnetic properties (**Fig. 7a**).

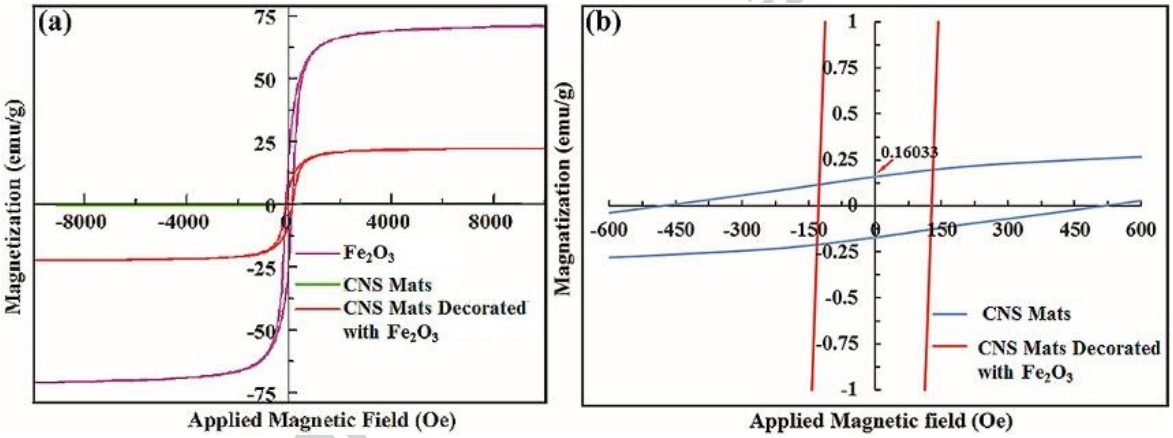

Fig. 6 (a) Magnetic hysteresis loop of pristine CNS mats, ɤ-Fe_2O_3 NPs decorated CNS mat, and γ-Fe_2O_3 NPs. (b) Enlarged magnetic hysteresis loop for CNS mats and ɤ-Fe_2O_3 NPs decorated CNS mat.

Furthermore, the remnant magnetization, M_r ~ 22.25 emu/g and the coercive field, H_C ~ 115.2 Oe of ɤ-Fe_2O_3 NPs indicate that the ɤ-Fe_2O_3 nanoparticles exhibited strong hard-magnetic properties [49]. ɤ-Fe_2O_3 NPs in CNS matrix resulted in an enhancement in the Hc~126 Oe, whereas the M_S decreased to 22.3 emu/g and the M_r decreased to 7.15 emu/g. Pristine CNS mats showed extremely high coercive fields (Hc~310 Oe) but very weak magnetization properties (0.23 emu/g), and this makes it unfavorable for electromagnetic (EM) wave absorption. ɤ-Fe_2O_3 NPs decorated CNS mats show superior magnetic properties compared to pristine CNS mats (M_S~22.3 emu/g, Hc~126 Oe) suggesting that it is an excellent candidate for enhanced EM

wave absorption. For applications in microwave absorption, higher magnetization value is favorable to the improvement of the initial permeability (μ_i) value as well as the final absorption. Initial permeability, μ_i, of ferromagnetic materials can be expressed as follows [23,50]:

$$\mu_i = \frac{M_s^2}{akH_cM_s + b\lambda\xi} \qquad (1)$$

Here, a and b are two constants determined by the material composition, λ is the magnetostriction constant, ζ is an elastic strain parameter of crystal, and k is a proportion coefficient. According to equation (1), ɤ-Fe_2O_3 NP decorated CNS mats are expected to have enhanced microwave absorption capability compared to pristine CNS mats. **Fig. 7b** shows EM wave absorption for pristine CNS mats and ɤ-Fe_2O_3 NPs decorated CNS mats. It confirms that γ-Fe_2O_3 NPs enhance microwave absorption capability in CNS mats, and can be attributed to the increase in μ_i value.

Table I. Magnetic properties obtained from VSM measurements

	γ-Fe_2O_3	CNS	Fe_2O_3-CNS
Coercivity, Hc (Oe)	115	310	126
Magnetization, Ms (emu/g)	71	0.23	22.3
Remanence, Mr (emu/g)	22.25	0.161	7.15
Squareness, Mr/Ms	0.31	0.7	0.32

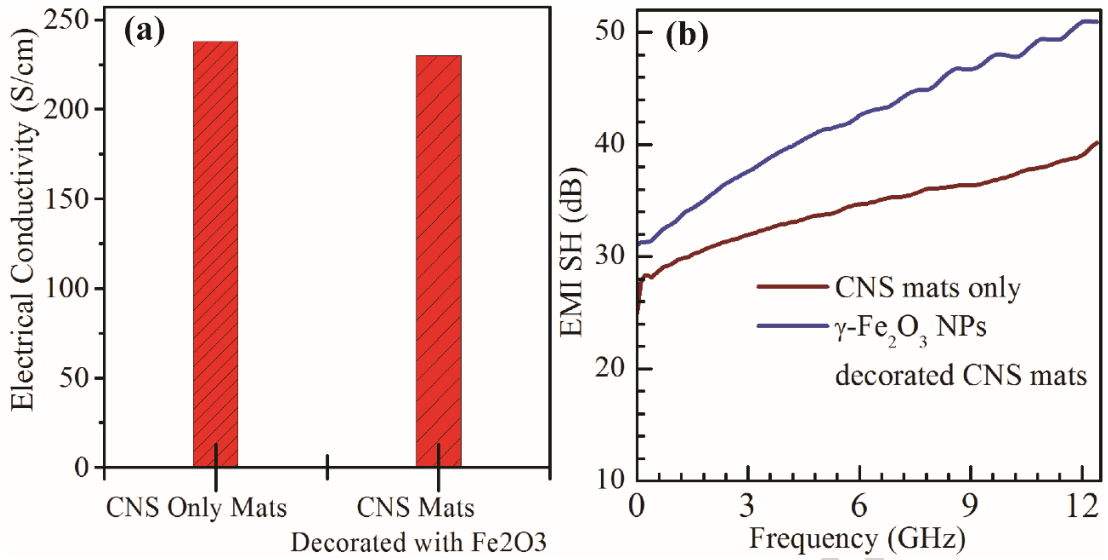

Fig. 7 (a) Electrical conductivity values for the CNS mat only and for the γ-Fe_2O_3 NPs decorated CNS mats, (b) Electromagnetic shielding absorption for the pristine CNS mat and magnetic sensitive CNS mats decorated with γ-Fe_2O_3 NPs.

4. Conclusions

In summary, a facile approach is demonstrated to fabricate a high electrical conductivity carbon-nanotube structure with enhanced magnetic properties, by embedding γ-Fe_2O_3 NPs in a 3D network structure consisting of CNS. We used SEM, AFM, TEM and VSM characterization to identify a 3D network structure of CNS with superior alignment, density and magnetic sensitivity. The as developed structure shows enhanced magnetic properties with saturation magnetization, M_S~22.3 emu/g, and coercive field, Hc~126 Oe. The structure is proposed to have a variety of promising applications such as electromagnetic shielding, sensors, lithium ion batteries, and polymer composites.

Acknowledgment

The authors are gratefully thanks Dr. Florent for his help with TEM images. Dr. Amal would like to thank Masdar Institute of Science and Technology for the financial support.

References

1. S. Iijima, *Nature* **354,** 56 (1991).
2. M. S. Dresselhaus, *Annual Rev. Mater. Sci.* **27,** 1 (1997).

3. L. Liu, A. H. Barber, S. Nuriel, and H. D. Wagner, *Adv. Funct. Mater.* **15,** 975 (2005).
4. S. Berber, Y. K. Kwon, and D. Tománek, *Phys. Rev. Lett.* **84,** 4613 (2000).
5. S. Hong and S. Myung, *Nat. Nanotechnology* **2,** 207 (2007).
6. T. Dürkop, S. Getty, E. Cobas, and M. Fuhrer, *Nano letters* **4,** 35 (2004).
7. R. H. Baughman, A. A. Zakhidov, and W. A. De Heer, *Science* **297,** 787 (2002).
8. M. S. Dresselhaus, *Nat. Mater.* **3,** 665 (2004).
9. H. Wang, L. Cao, S. Yan, N. Huang, and Z. Xiao, *Mater. Sci. Eng.: B* **164,** 191 (2009).
10. E. Camponeschi, R. Vance, M. Al-Haik, H. Garmestani, and R. Tannenbaum, *Carbon* **45,** 2037 (2007).
11. Q. Liao, J. Sun, and L. Gao, *Colloids and Surfaces A: Physicochemical and Engineering Aspects* **345,** 95 (2009).
12. P. Gonnet, Z. Liang, E. S. Choi, R. S. Kadambala, C. Zhang, J. S. Brooks, B. Wang, and L. Kramer, *Curr. Appl. Phys.* **6,** 119 (2006).
13. N. F. Colaneri and L. Schacklette, *IEEE transactions on instrumentation and measurement* **41,** 291 (1992).
14. N. Das, D. Khastgir, T. Chaki, and A. Chakraborty, *Composites part A: applied science and manufacturing* **31,** 1069 (2000).
15. R. Che, C. Zhi, C. Liang, and X. Zhou, *Appl. Phys. Lett.* **88,** 033105 (2006).
16. M.-S. Cao, X. L. Shi, X. Y. Fang, H. B. Jin, Z. L. Hou, W. Zhou, and Y. J. Chen, *Appl. Phys. Lett.* **91,** 203110 (2007).
17. D. Liu, J. Zhu, S. Ivaturi, Y. He, S. Wang, J. Wang, S. Zhang, M. A. Willis, and F. S. Boi, *RSC Adv.* **8,** 13820 (2018).
18. H. Terrones, F. López-Urías, E. Munoz-Sandoval, J. Rodríguez-Manzo, A. Zamudio, A. Elías, and M. Terrones, *Solid state sciences* **8,** 303 (2006).
19. J. Zhu, D. Liu, J. Wang, H. Yi, S. Wang, J. Wen, M. Willis, Y. Hou, J. Borowiec, and F. Boi, *RSC Adv.* **7,** 20604 (2017).
20. J. Guo, M. Lan, S. Wang, Y. He, S. Zhang, G. Xiang, and F. S. Boi, *Phys. Chem. Chem. Phys.* **17,** 18159 (2015).
21. G. Korneva, H. Ye, Y. Gogotsi, D. Halverson, G. Friedman, J. C. Bradley, and K. G. Kornev, *Nano letters* **5,** 879 (2005).
22. X. Wang, Z. Zhao, J. Qu, Z. Wang, and J. Qiu, *J. Phys. Chem. Solids* **71,** 673 (2010).
23. R. Lv, A. Cao, F. Kang, W. Wang, J. Wei, J. Gu, K. Wang, and D. Wu, *J. Phys. Chem. C* **111,** 11475 (2007).
24. N. Kiselev, R. Zakalyukin, O. Zhigalina, N. Grobert, A. Kumskov, Y. V. Grigoriev, M. Chernysheva, A. Eliseev, A. Krestinin, and Y. D. Tretyakov, *J. Microscopy* **232,** 335 (2008).
25. H. Younes, R. A. Al-Rub, M. M. Rahman, A. Dalaq, A. Al Ghaferi, and T. Shah, *Diamond and Related Mater.* **68,** 109 (2016).
26. M. M. Rahman, H. Younes, N. Subramanian, and A. A. Ghaferi, *J. Nanomaterials* **2014,** 145 (2014).
27. M. Islam, E. Rojas, D. Bergey, A. Johnson, and A. Yodh, *Nano letters* **3,** 269 (2003).

28. H. Hong, X. Luan, M. Horton, C. Li, and G. Peterson, *Thermochimica Acta* **525,** 87 (2011).
29. L. Hu, J. W. Choi, Y. Yang, S. Jeong, F. La Mantia, L. F. Cui, and Y. Cui, *Proceedings of the National Academy of Sciences* **106,** 21490 (2009).
30. J. W. Kang, K. S. Kim, and H. J. Hwang, *Computational Mater. Sci.* **50,** 1818 (2011).
31. Z. Ai, Y. Wang, M. Xiao, L. Zhang, and J. Qiu, *J. Phys. Chem. C* **112,** 9847 (2008).
32. P. Feng, X. b. Fu, Y. Hao, and H. J. Wang, *New Carbon Mater.* **22,** 213 (2007).
33. A. Masotti and A. Caporali, *International journal of molecular sciences* **14,** 24619 (2013).
34. H. Gul, W. Lu, P. Xu, J. Xing, and J. Chen, *Nanotechnology* **21,** 155101 (2010).
35. M. Zhang, Y. Wang, Y. Zhang, L. Ding, J. Zheng, and J. Xu, *Appl. Surf. Sci.* **375,** 154 (2016).
36. E. T. Thostenson and T. W. Chou, *J. Phys. D: Appl. Phys.* **35,** L77 (2002).
37. M. S. Mauter, M. Elimelech, and C. O. Osuji, *Acs Nano* **4,** 6651 (2010).
38. I. T. Kim, A. Tannenbaum, and R. Tannenbaum, *Carbon* **49,** 54 (2011).
39. G. Christensen, H. Younes, H. Hong, and G. Peterson, *J. Nanofluids* **2,** 25 (2013).
40. H. Younes, G. Christensen, M. Liu, H. Hong, Q. Yang, and Z. Lin, *J. Nanofluids* **3,** 33 (2014).
41. C. Gao, W. Li, H. Morimoto, Y. Nagaoka, and T. Maekawa, *J. Phys. Chem. B* **110,** 7213 (2006).
42. Y. Li, Y. Huang, S. Qi, L. Niu, Y. Zhang, and Y. Wu, *Appl. Surf. Sci.* **258,** 3659 (2012).
43. Y. Guan, C. Jiang, C. Hu, and L. Jia, *Talanta* **83,** 337 (2010).
44. L. Gao and L. Chen, *Microchimica Acta* **180,** 423 (2013).
45. T. K. Shah, B. W. Pietras, D. J. Adcock, H. C. Malecki, and M. R. Alberding, (*Google Patents*, 2013).
46. H. Younes, R. A. Al-Rub, M. Mahfuzur Rahman, A. Dalaq, A. Al Ghaferi, and T. Shah, *Diamond and Related Mater.* **68,** 109 (2016).
47. H. Younes, G. Christensen, X. Luan, H. Hong, and P. Smith, *J. Appl. Phys.* **111,** 064308 (2012).
48. S. H. Lee, D. Kang, and I. K. Oh, *Carbon* **111,** 248 (2017).
49. M. W. Kim, W. J. Han, Y. H. Kim, and H. J. Choi, *Colloids and Surfaces A: Physicochemical and Engineering Aspects* **506,** 812 (2016).
50. J. Fang, T. Liu, Z. Chen, Y. Wang, W. Wei, X. Yue, and Z. Jiang, *Nanoscale* **8,** 8899 (2016).